Chemical Engineering Science 108 (2014) 9–22

Contents lists available at ScienceDirect

Chemical Engineering Science

journal homepage: www.elsevier.com/locate/ces

Numerical study of bubble break-up in bubbly flows using a deterministic Euler–Lagrange framework

Y.M. Lau, W. Bai, N.G. Deen *, J.A.M. Kuipers

Multiphase Reactors Group, Department of Chemical Engineering and Chemistry, Eindhoven University of Technology, P.O. Box 513, 5600 MB, Eindhoven, The Netherlands

HIGHLIGHTS

- A simulation framework for heterogeneous bubbly flow is presented.
- A Lagrangian breakup model is proposed.
- The daughter size distribution does not influence the bubble size distribution (BSD).
- The critical Weber number and superficial gas velocity significantly affect the BSD.

GRAPHICAL ABSTRACT

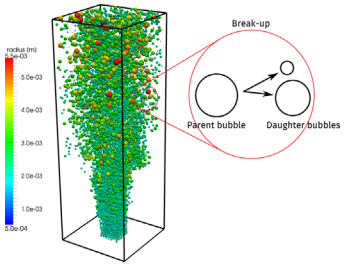

ARTICLE INFO

Article history:
Received 26 July 2013
Received in revised form
26 November 2013
Accepted 23 December 2013
Available online 2 January 2014

Keywords:
Euler–Lagrange model
Bubble columns
Coalescence
Break-up
Daughter size distribution

ABSTRACT

In this work we present a numerical model to predict the bubble size distribution in turbulent bubbly flows. The continuous phase is described by the volume-averaged Navier–Stokes equations, which are solved on an Eulerian grid, whereas the dispersed or bubble phase is treated in a Lagrangian manner, where each individual bubble is tracked throughout the computational domain. Collisions between bubbles are described by means of a hard-sphere model. Coalescence of bubbles is modeled via a stochastic inter-particle encounter model. A break-up model is implemented with a break-up constraint on the basis of a critical Weber value augmented with a model for the daughter size distribution. A numerical parameter study is performed of the bubble break-up model implemented in the deterministic Euler–Lagrange framework and its effect on the bubble size distribution (BSD) is reported. A square bubble column operated at a superficial gas velocity of 2 cm/s is chosen as a simulation base case to evaluate the parameters. The parameters that are varied are the values of the critical Weber number (We_{crit}), the daughter size distribution (β) and the superficial gas velocity (v_{sup}). Changes in the values of We_{crit} and v_{sup} have a significant impact on the overall BSD, while a different shaped β did not show a significant difference.

1. Introduction

In turbulent bubbly flows, coalescence and break-up of bubbles determine the bubble size distribution and the corresponding interfacial area. Hence, these phenomena play a crucial role in mass and heat transfer operations in bubbly flows. To predict the bubble size distribution in industrial bubbly flows, the population balance equation (PBE) embedded in the Euler–Euler model is often used. Traditionally the Euler–Euler model treats the dispersed gas phase as a separate continuum with averaged properties, i.e. mean bubble diameter. The disadvantage is that the information regarding individual bubbles is not available. To retain the bubble size distribution a PBE is employed. The PBE handles the evolution of the size distribution of the dispersed phase

* Corresponding author.
E-mail address: N.G.Deen@tue.nl (N.G. Deen).

0009-2509/$ - see front matter © 2014 Elsevier Ltd. All rights reserved.
http://dx.doi.org/10.1016/j.ces.2013.12.034

statistically through coalescence and break-up models. The PBE or number density transport equation considers bubbles entering and leaving a control volume through different mechanisms, such as convection, break-up/coalescence or evaporation/condensation. Many mathematical models presented in the literature for coalescence and break-up of bubbles (or droplets) are derived for the use in the PBE. Lasheras et al. (2002) and Liao and Lucas (2009) have given excellent reviews of literature break-up models; and Liao and Lucas (2010) for coalescence models.

Contrary to the classical Euler–Euler model, Euler–Lagrange models offer the advantage that the bubble size distribution is produced as part of the solution, provided that appropriate coalescence and break-up models are incorporated. Sungkorn et al. (2012) belong to the very few, who adopted the Euler–Lagrange framework to study the bubble size distribution (BSD). In their model, bubble parcels are treated in a Lagrangian manner, employing the break-up model of Prince and Blanch (1990) and the coalescence model of Luo and Svendsen (1996). Instead of bubble parcels, Darmana et al. (2006) tracked individual bubbles and treats coalescence in a deterministic fashion after contact of two individual bubbles. The proposed coalescence model is based on the stochastic model of Sommerfeld et al. (2003) whereas break-up of individual bubbles was not incorporated. Building upon the work of Darmana et al. (2006), a deterministic Euler–Lagrange model is presented in this chapter along with the implementation of a bubble break-up model. Similar to coalescence models, incorporation of break-up models originally developed for PBE models in the Euler–Lagrange model is not straightforward. This is due to differences in the mathematical representation, however the underlying physics to represent these phenomena will still hold. The associated constraints can still be used to formulate criterions for coalescence and break-up in the Euler–Lagrange model. Coalescence models for the PBE are given in terms of a coalescence frequency:

$$\Theta_{co}(d_i,d_j)=h_{coll}(d_i,d_j)\gamma_{co}(d_i,d_j) \tag{1}$$

where $h_{coll}(d_i,d_j)$ is the collision frequency between two bubbles with diameters of d_i and d_j; and $\gamma_{co}(d_i,d_j)$ is the corresponding coalescence efficiency. In the Euler–Lagrange framework the collision frequency is readily available. So, using the underlying premise of the coalescence efficiency, a coalescence constraint can be derived for the use in the Euler–Lagrange framework. Such is the coalescence model in the current framework proposed by Darmana et al. (2006). However, coalescence models for the PBE do not give information regarding the location of the resulting coalesced bubble and an assumption must be made regarding the positioning of the newly formed bubble.

Similar to the coalescence frequency, the break-up frequency for the PBE is given as

$$\Theta_{bu}(d_i)=h_{bu}(d_i)\gamma_{bu}(d_i) \tag{2}$$

where $h_{bu}(d_i)$ is the arrival frequency of eddies interacting with a bubble and $\gamma_{bu}(d_i)$ is the break-up efficiency. In the Euler–Lagrange framework, the underlying premise of the break-up efficiency can be used as a break-up constraint. To complete the break-up model, we need a size distribution $\beta(d_i)$ of daughter bubbles formed from the break-up of a parent bubble of size d_i. Also, the locations of the resulting daughter bubbles are not given and assumptions are to be made concerning the placement of the daughter bubbles after the break-up event.

In the following sections, the Euler–Lagrange model and the implemented coalescence model will be described. A break-up model based on the constraint of a critical Weber value is proposed along with the daughter size distribution. Subsequently the numerical implementation of the model in the Euler–Lagrange framework is described. And finally, we present a numerical parameter study of the break-up model implemented in the Euler–Lagrange framework and the effect on the resulting BSD.

2. Euler–Lagrange model

In the Euler–Lagrange model, each individual bubble is treated in a Lagrangian manner, while the liquid phase motion is computed on an Eulerian grid, taking into account the coupling or interaction between the gas and the liquid phase. Bubble–bubble collisions are modeled by means of a hard sphere model following the work of Hoomans et al. (1996) and Delnoij et al. (1997, 1999).

2.1. Liquid phase hydrodynamics

The liquid phase is represented by the volume-averaged Navier–Stokes equations, defined by the continuity and momentum equations:

$$\frac{\partial}{\partial t}(\alpha_l\rho_l)+\nabla\cdot\alpha_l\rho_l\mathbf{u}=0 \tag{3}$$

$$\frac{\partial}{\partial t}(\alpha_l\rho_l\mathbf{u})+\nabla\cdot\alpha_l\rho_l\mathbf{u}\mathbf{u}=-\alpha_l\nabla P-\nabla\cdot\alpha_l\tau_l+\alpha_l\rho_l\mathbf{g}+\Phi \tag{4}$$

The presence of the bubbles is reflected by the liquid phase volume fraction α_l and the interphase momentum transfer rate Φ due to the interface forces between the liquid and the bubbles. The liquid phase flow is assumed to be Newtonian and a subgrid-scale model by Vreman (2004) is employed for the turbulence. In an earlier study Darmana et al. (2007) have compared the model by Vreman (2004) to the model by Smagorinsky (1963). It was decided to use by Vreman (2004) model rather than the Smagorinsky (1963) model, as it inherently accounts for the reduction of the energy dissipation in near-wall regions.

2.2. Bubble dynamics

The bubble motion is obtained by solving Newton's second law for each individual bubble. The forces are taken into account by the net force $\sum\mathbf{F}$, experienced by each individual bubble. Then the equations of motion are written as

$$\rho_g V_b\frac{d\mathbf{v}}{dt}=\sum\mathbf{F},\quad \frac{d\mathbf{r}_b}{dt}=\mathbf{v} \tag{5}$$

where $\mathbf{v}$ is the velocity, V_b is the volume and $\mathbf{r}_b$ is the bubble location of the bubble. The net force acting on each individual bubble is assumed to consist of separate and uncoupled distributions originating from gravity, far field pressure, drag, lift, virtual mass and wall-interaction:

$$\sum\mathbf{F}=\mathbf{F}_G+\mathbf{F}_P+\mathbf{F}_D+\mathbf{F}_L+\mathbf{F}_{VM}+\mathbf{F}_W \tag{6}$$

To close the force balance equation, correlations are needed for the drag (Roghair et al., 2011), lift (Tomiyama et al., 2002), virtual mass (Auton, 1987) and wall-interaction (Tomiyama et al., 1995). These are listed in Table 1. Details on the forces and the numerical implementation are given in the work of Darmana et al. (2006). It should be noted that Euler–Lagrange model is limited by the shape of the bubble, which is in this case assumed to be spherical.

3. Coalescence model

For the description of the coalescence process, three main theories have been proposed, the kinetic collision model (Howarth, 1964; Sovova, 1981), the film drainage model (Sagert and Quinn, 1976; Lee et al., 1987; Prince and Blanch, 1990; Chesters, 1991; Tsouris and Tavlarides, 1994) and the critical velocity model (Lehr et al., 2002). In the kinetic collision or

Table 1
Overview of forces acting on a bubble.

Force		Closure
$\mathbf{F}_G = \rho_g \mathbf{g} V_b$	(7)	–
$\mathbf{F}_P = -V_b \nabla P$	(8)	–
$\mathbf{F}_D = -\frac{1}{2} C_D \rho_l \pi R_b^2 \lvert\mathbf{v}-\mathbf{u}\rvert(\mathbf{v}-\mathbf{u})$	(9)	$\frac{C_D}{C_{D,\infty}} = \left(1+\frac{18}{\mathrm{E\ddot{o}}}\alpha_g\right)\alpha_l$ $C_{D,\infty} = \sqrt{C_{D,\infty}(\mathrm{Re})^2 + C_{D,\infty}(\mathrm{E\ddot{o}})^2}$ $C_{D,\infty}(\mathrm{Re}) = \frac{16}{\mathrm{Re}}\left(1+\frac{2}{1+\frac{16}{\mathrm{Re}}+\frac{3.315}{\sqrt{\mathrm{Re}}}}\right)$ $C_{D,\infty}(\mathrm{E\ddot{o}}) = \frac{4\mathrm{E\ddot{o}}}{\mathrm{E\ddot{o}}+9.5}$
$\mathbf{F}_L = -C_L \rho_l V_b (\mathbf{v}-\mathbf{u}) \times (\nabla \times \mathbf{u})$	(10)	$C_L = \begin{cases} \min[0.288\tanh(0.121\mathrm{Re}), f(\mathrm{E\ddot{o}}_d)] & \mathrm{E\ddot{o}} < 4 \\ f(\mathrm{E\ddot{o}}_d) & 4 < \mathrm{E\ddot{o}} \le 10 \\ -0.29 & \mathrm{E\ddot{o}} > 10 \end{cases}$ $f(\mathrm{E\ddot{o}}_d) = 0.00105\mathrm{E\ddot{o}}_d^3 - 0.0159\mathrm{E\ddot{o}}_d^2 - 0.0204\mathrm{E\ddot{o}}_d + 0.474$ $\mathrm{E\ddot{o}}_d = \frac{\mathrm{E\ddot{o}}}{E_b}, \quad E_b = \frac{1}{1+0.163\mathrm{E\ddot{o}}^{0.757}}$
$\mathbf{F}_{VM} = -\left(C_{VM}\rho_l V_b \frac{D(\mathbf{v}-\mathbf{u})}{Dt} + C_{VM}\rho_l V_b (\mathbf{v}-\mathbf{u})\cdot\nabla\mathbf{u}\right)$	(11)	$C_{VM} = 0.5$
$\mathbf{F}_W = -C_W \frac{d}{2}\left[\frac{1}{y^2} - \frac{1}{(L-y)^2}\right]\rho_l \lvert(\mathbf{v}-\mathbf{u})\cdot\mathbf{n}_z\rvert^2 \mathbf{n}_w$	(12)	$C_W = \begin{cases} e^{(-0.933\mathrm{E\ddot{o}}+0.179)} & 1 \le \mathrm{E\ddot{o}} \le 5 \\ 0.007\mathrm{E\ddot{o}}+0.04 & 5 < \mathrm{E\ddot{o}} \le 33 \end{cases}$

energetic model, the coalescence process is governed by the impact of the collision of the bubbles. If the approach velocity of the two colliding bubbles at the instant of the collision event exceeds a critical value, the two bubbles will coalesce. In the film drainage model, the coalescence process is divided into three steps: (1) two bubbles collide and trap a small amount of liquid between them; (2) while both bubbles stay in contact, the liquid film drains out to a critical thickness and (3) ruptures, leading to the bubbles to coalesce. The constraint here for coalescence to occur is that the duration of the contact time of the bubbles must be sufficiently long for the liquid film to drain. The critical velocity model postulates that the approach velocities of both bubbles must be small enough to lead to the coalescence of the bubbles.

To illustrate the possibility to use the underlying constraints of the literature coalescence models in the Euler–Lagrange framework, two example cases are given below, i.e. the kinetic collision model by Howarth (1964) and the film drainage model by Chesters (1991). In the example cases the coalescence efficiency is written as a coalescence constraint. As the first example case, Howarth (1964) considered the collision of two droplets and proposed that coalescence will occur when the approach velocity at the instant of collision exceeds a critical value. These collisions are called energetic collisions. The surface energy of the droplets is proportional to the surface tension and surface area:

$$E_s = \sigma\left(\frac{\pi}{6}\right)^{2/3}(d_1^2+d_2^2) \tag{13}$$

The kinetic energy is assumed to be proportional to the average volume $\overline{V}$ and the relative velocity of two colliding drops v_{rel}:

$$E_{\mathrm{kin}} = \frac{1}{2}\rho_g v_{rel}^2 \frac{\pi}{6}\frac{d_1^3 d_2^3}{d_1^3+d_2^3} \tag{14}$$

The relative velocity between two droplets of size d_1 and d_2 is proportional to the mean-square root of the two velocities v_1 and v_2:

$$v_{rel} = \sqrt{(v_1^2+v_2^2)} \tag{15}$$

For coalescence to occur, the kinetic collision energy must exceed the surface energy:

$$E_{\mathrm{kin}} > E_s \tag{16}$$

Written in a dimensionless Weber form, this constraint is

$$\frac{\rho_g v_{rel}^2 \overline{d}}{\sigma} > 2\left(\frac{\pi}{6}\right)^{-1/3} \tag{17}$$

with $\overline{d} = (d_1^3 d_2^3)/((d_1^2+d_2^2)(d_1^3+d_2^3))$.

The second example case is the film drainage model by Chesters (1991). For coalescence to occur, the contact time must exceed the film drainage (or coalescence) time of the bubbles:

$$t_{\mathrm{contact}} \ge t_{\mathrm{drainage}} \tag{18}$$

The following relation is used for the calculation of the film drainage time:

$$t_{\mathrm{drainage}} = \frac{3\mu_c F_{coll}}{8\pi\sigma^2} d_{eq}\left(\frac{1}{\theta_f^2}-\frac{1}{\theta_0^2}\right) \tag{19}$$

where the θ_0 is the initial film thickness and θ_f the final film thickness just before film drainage. The equivalent bubble diameter for a system of two different sized bubbles is obtained from

$$d_{eq} = \left(\frac{1}{d_1}+\frac{1}{d_2}\right)^{-1} \tag{20}$$

The force F_{coll} is the collision force between the bubbles and is given by Coulaloglou and Tavlarides (1977) and Tsouris and Tavlarides (1994) as

$$F_{coll} \sim \rho_l \varepsilon^{2/3}(d_1+d_2)^{2/3} d_{eq}^2 \tag{21}$$

Chesters (1991) derived for the contact time the following relation:

$$t_{\mathrm{contact}} \approx \left(\frac{\left(\frac{4\rho_g}{3\rho_l}+1\right)\rho_l d_{eq}^3}{16\sigma}\right)^{1/2} \tag{22}$$

Since the collision frequency is readily available in the Euler–Lagrange model, the coalescence constraints of the example cases, Eqs. (16) and (18) can be evaluated for each bubble–bubble encounter. In this work we use the film drainage model as implemented by Darmana et al. (2006). For the drainage time the relation of Prince and Blanch (1990) is used:

$$t_{\text{drainage}} = \sqrt{\frac{d_{eq}^3 \rho_l}{128\sigma}} \ln\left(\frac{\theta_0}{\theta_f}\right) \tag{23}$$

According to Sommerfeld et al. (2003), the contact time between two bubbles is calculated by assuming that it is proportional to a deformation distance divided by the normal component of the collision velocity:

$$t_{\text{contact}} = \frac{C_{co} d_{eq}}{2|\mathbf{v}_1^N - \mathbf{v}_2^N|} \tag{24}$$

where the coalescence constant (C_{co}) represents the deformation distance normalized by the effective bubble diameter. The criteria for the occurrence of coalescence or collision (and bounce off) are determined by the ratio of the contact time and the film drainage time $t_{\text{contact}}/t_{\text{drainage}}$. Written in a dimensionless Weber form, this constraint is

$$\text{We} = \frac{\rho_l (\mathbf{v}_1^N - \mathbf{v}_2^N)^2 d_{eq}}{\sigma} \leq 2 \cdot \left(\frac{4C_{co}}{\ln\left(\frac{\theta_0}{\theta_f}\right)}\right)^2 \tag{25}$$

4. Break-up model

Break-up mechanisms can be classified into four main categories regarding the governing physical process: turbulent fluctuation and collision; viscous shear stress; shearing off process and interfacial instability. From these mechanisms, bubble break-up due to turbulent pressure fluctuation along the surface or by collision with eddies has been investigated most extensively. This mechanism is assumed to be the dominant break-up mechanism in our case involving turbulent bubbly flows.

Concerning the break-up criteria itself, four different criteria have been reported in the literature. The associated critical values involve the turbulent kinetic energy of the bubble (Coulaloglou and Tavlarides, 1977; Chatzi et al., 1989; Chatzi and Kiparissides, 1992), the velocity fluctuation around the bubble surface (Narsimhan and Gupta, 1979; Alopaeus et al., 2002), the turbulent kinetic energy of the impacting eddy (Lee et al., 1987; Prince and Blanch, 1990; Tsouris and Tavlarides, 1994; Luo and Svendsen, 1996; Martínez-Bazán et al., 1999) and the inertial force of the impacting eddy (Lehr et al., 2002). According to these models, if each one of the mentioned energies or forces exceeds the critical value, the bubble breaks up. In the following section, we will show that the above-mentioned models can be written in terms of a critical Weber number. This critical Weber number can subsequently be used as a break-up constraint for an individual bubble.

4.1. Break-up constraint

4.1.1. Literature models for break-up criteria

Hinze (1955) is one of the first to establish a break-up theory by introducing a dimensionless ratio between the inertial force (which causes deformation) and the surface tension (which tends to restore the bubble sphericity). In turbulent flows the deformation is induced by inertia and the dimensionless number is known as the Weber number:

$$\text{We} = \frac{\rho \overline{\delta u^2(d)} d}{\sigma} \tag{26}$$

where ρ_l is the density of the continuous phase and $\overline{\delta u^2(d)}$ is the mean square velocity difference over a distance equal to the bubble diameter. Assuming isotropic turbulence (Kolmogorov, 1949; Batchelor, 1951), the Weber number can also be written as

$$\text{We} = \frac{c_1 \rho \varepsilon^{2/3} d^{5/3}}{\sigma} \tag{27}$$

In this subsection, the break-up constraints of selected literature models are described and it is shown that all constraints can be written in the form of a dimensionless Weber number.

Coulaloglou and Tavlarides (1977) derived their break-up model for droplets, but many researchers have applied it as well for the break-up of bubbles. In their model, the basic premise is that an oscillating bubble will break-up if the turbulent kinetic energy transmitted to the bubble by the turbulent eddies exceeds the bubble surface energy. The bubble surface energy is given as

$$E_s = c_2 \sigma d^2 \tag{28}$$

With the assumption that the kinetic energy distribution of the droplet is the same as that of the eddies, the mean turbulent kinetic energy is given as

$$E_t = c_3 \rho d^3 \overline{u^2(d)} = c_4 \rho \varepsilon^{2/3} d^{11/3} \tag{29}$$

Therefore, the break-up of a droplet occurs if its turbulent kinetic energy E_t exceeds the droplet surface energy E_s:

$$\text{We}_{\text{crit}} = \frac{\rho \varepsilon^{2/3} d^{5/3}}{\sigma} \geq \frac{c_2}{c_4} \tag{30}$$

Originally the density chosen in the above formulation was the dispersed phase density (Coulaloglou and Tavlarides, 1977), which in the case of bubbly flow corresponds to the gas density. However, Lasheras et al. (2002) pointed out that the density of the continuous phase should be used, which is the liquid phase for bubbly flow.

Narsimhan and Gupta (1979) derived a break-up model for droplets in liquid–liquid dispersions. They postulated that for the occurrence of break-up, the kinetic energy $1/2u_\lambda^2$ of the eddy with a length scale λ arriving at the droplet surface must exceed the minimum increase of the surface energy for binary break-up, $1/2u_\lambda^2 \geq 1/2u_{\min}^2$ respectively. The arriving eddies cause the droplet to oscillate and break-up. Hence, the minimum increase of the surface energy for binary break-up is provided by the kinetic energy of the oscillation of the droplet:

$$\frac{1}{2}\left(\rho\left(\frac{\pi}{6}d^3\right)\right) u_{\min}^2 = (2^{1/3} - 1)\sigma\pi d^2 \tag{31}$$

This leads to the following break-up constraint:

$$\text{We}_{\text{crit}} = \frac{\rho u_\lambda^2 d}{\sigma} \geq 12(2^{1/3} - 1) = 3.12 \tag{32}$$

As the break-up constraint, most statistical models employ the criterion of the turbulent kinetic energy of the impacting eddy exceeding a critical value. Prince and Blanch (1990) used a critical Weber value of 2.3 for air bubbles in water for the formulation of their break-up model. Another popular model was proposed without any model parameters by Luo and Svendsen (1996). They defined the increase in surface energy during break-up as the critical value using the daughter size distribution for the

formulation of the break-up constraint:

$$\mathrm{We}_{\mathrm{crit}} = \frac{\rho_l \varepsilon^{2/3} d^{5/3}}{\sigma} \geq \frac{12 c_f}{c_5 \left(\frac{\lambda}{d}\right)^{11/3}} \tag{33}$$

with $c_f = f_{bv}^{2/3} + (1 - f_{bv})^{2/3}$ and the volumetric break-up fraction $f_{bv} = V_1/V_0$.

Martínez-Bazán et al. (1999) developed a model for the break-up of an air bubble in a fully developed turbulent water flow. They postulated that when the turbulent stresses from the velocity fluctuations exceed the surface restoring pressure of the bubble, the bubble will deform and eventually break-up. The surface restoring pressure of a bubble with a size d is

$$\tau_s(d) = 6\frac{\sigma}{d} \tag{34}$$

The average deformation force per unit surface produced by the turbulent stresses resulting from the velocity fluctuations existing in the liquid between two points separated by a distance d can be estimated as

$$\tau_t(d) = \frac{1}{2} c_6 \rho (\varepsilon d)^{2/3} \tag{35}$$

The equality of both stresses defines the critical bubble diameter $d_{b,\mathrm{crit}}$, such that bubbles with $d_b < d_{b,\mathrm{crit}}$ are stable and will never break. Thus for break-up to occur, the following must be valid:

$$\mathrm{We}_{\mathrm{crit}} = \frac{\rho \varepsilon^{2/3} d^{5/3}}{\sigma} \geq \frac{12}{c_6} \tag{36}$$

Lehr et al. (2002) proposed to use the interfacial force of the smallest daughter bubble as the critical value for inertial force of the impacting turbulent eddy:

$$\mathrm{We}_{\mathrm{crit}} = \frac{\rho_l u_\lambda d_{\text{smallest daughter}}}{\sigma} \geq 4 \tag{37}$$

Using the assumption that only eddies with length scales smaller than the bubble diameter can induce break-up, the following relation is obtained:

$$d_{\text{smallest daughter}} \leq \lambda \leq d \tag{38}$$

where λ is the length scale of the eddy and d is the parent bubble diameter. This model has the same advantage as the model by Luo and Svendsen (1996) that the daughter bubble distribution is incorporated in the break-up constraint.

As shown in the above relations, on the basis of literature break-up models, a break-up constraint can be established in the form of the dimensionless Weber number. Many of these models require experiments to acquire the critical value. Some of the experimentally acquired critical Weber values for specific systems are given in Table 1.

4.1.2. Break-up constraint in the Euler–Lagrange framework

Following a similar derivation as Martínez-Bazán et al. (1999), a break-up constraint is established for the Euler–Lagrange framework. Hence the basic premise of the break-up model is that for the bubble to break, its surface has to deform, and this deformation energy is provided by the turbulent stresses produced by the surrounding liquid. The minimum energy necessary to deform a spherical bubble of size d is its surface energy:

$$E_s = \sigma \pi d^2 \tag{39}$$

where σ is the surface tension. To account for non-spherical bubble shapes in the determination of the critical Weber number, the surface area of the non-spherical bubble must be incorporated. Using the aspect ratio E_b and the Eötvos number (Eö), the surface energy of a bubble with an equivalent bubble diameter d can be written as

$$E_s = \sigma \pi d^2 \cdot \zeta^{-1} \tag{40}$$

with

$$\zeta = \left(\frac{1 + 2E_b^p}{3E_b^{2/3p}}\right)^{-1/p} \tag{41}$$

where $p = 1.6075$ and $E_b = f(\mathrm{Eö})$. The surface area correction factor ζ is valid for Eövös < 40 and Morton $\leq 10^{-6}$. In Fig. 1 ζ is given as a function of the Eötvös number and the aspect ratio E_b. Details of the underlying derivation are given in the appendix. For spherical bubbles ζ becomes 1.

If viscous forces can be neglected in comparison with the surface tension forces (which means the Ohnesorge number $(\mu_g/\sqrt{\rho_g \sigma d})$ must be very small, $\mathrm{Oh} < 10^{-2}$), the confinement stress or surface restoring pressure is

$$\tau_s(d) = \frac{E_s}{V_b} = \frac{6E_s}{\pi d^3} = 6\frac{\sigma}{d} \cdot \zeta \tag{42}$$

Assuming that the size of the bubble is within the inertial subrange, the average deformation stress, which results from velocity fluctuations existing in the liquid between two points separated by a characteristic distance, can be estimated as

$$\tau_t = \frac{1}{2} \rho_l \overline{\delta u^2(d)} \tag{43}$$

where ρ is the density of the continuous (liquid) phase and $\overline{\delta u^2(d)}$ is the average value of the square of the velocity differences over a characteristic distance d. When $\tau_t > \tau_s$, the bubble deforms and

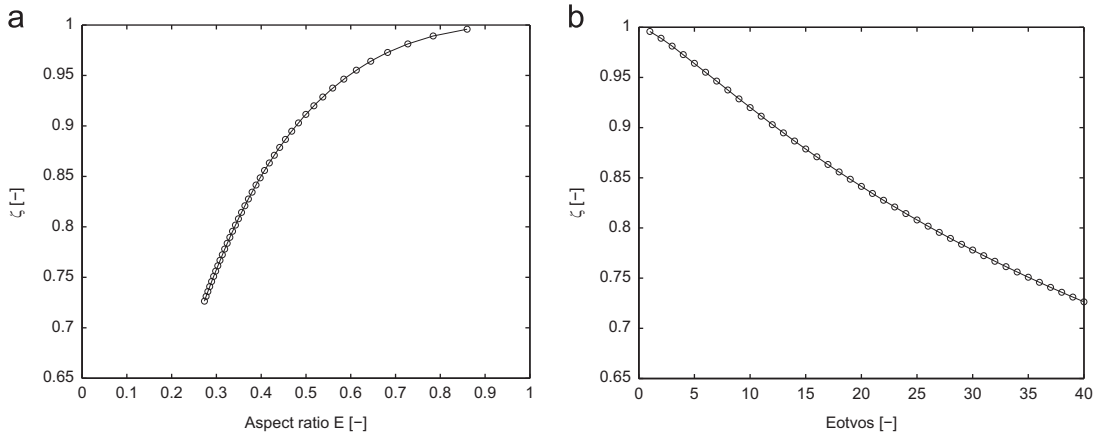

Fig. 1. The surface correction factor ζ as a function of (a) the Eötvös number and (b) the aspect ratio E_b.

eventually breaks up. The equality $\tau_t(d)=\tau_s(d)$, defines a critical Weber number, such that the bubble is just stable and does not break up:

$$\frac{\rho_l\overline{\delta u^2(d)}d}{\sigma}=12\cdot\zeta \tag{44}$$

Hence, the criterion for bubble break-up is defined as

$$We\geq 12\zeta \tag{45}$$

4.2. Daughter size distribution

Most break-up models reported in the literature assume binary break-up and the size of daughter bubbles is determined by the break-up volume fraction f_{bv}. For a few models, the f_{bv} is directly linked to the break-up constraint, such as in the break-up model by Luo and Svendsen (1996). The break-up fraction is a random variable, either based on empirical observations or acquired from a statistical distribution (uniform, normal and beta). By categorizing the daughter size distributions on the basis of their shape, the following daughter size distributions can be distinguished (also see Fig. 2):

- Uniform distribution (Narsimhan and Gupta, 1979; Prince and Blanch, 1990): The parent bubble can break up in daughter bubbles of any size with an equal probability.

$$f_{bv}=\Upsilon \tag{46}$$

  where Υ is a random value between 0 and 1.
- Bell-shape or normal distribution (Martínez-Bazán et al., 1999; Lee et al., 1987): Daughter bubbles with equal size have the highest probability to occur, while one large and one small daughter bubble have less probability.

$$f_{bv}(\Upsilon)=\frac{\Gamma(4)}{\Gamma(2)\Gamma(2)}\Upsilon(1-\Upsilon) \tag{47}$$

  where Γ is the gamma function.
- U-shape (Luo and Svendsen, 1996; Tsouris and Tavlarides, 1994): The probability that a small daughter bubble breaks off from the parent bubble is the highest and equal size break-up has the lowest probability.

$$f_{bv}(\Upsilon)=\frac{\Gamma(1)}{\Gamma(0.5)\Gamma(0.5)}\Upsilon^{-1/2}(1-\Upsilon)^{-1/2} \tag{48}$$

- M-shape (Lehr et al., 2002): Neither equal size break-up nor a small daughter bubble break off has a high probability, but break-up values in between these two extremes have the highest probability.

$$f_{bv}(\Upsilon)=\frac{\Gamma(4)}{\Gamma(2)\Gamma(2)}\Upsilon(1-\Upsilon) \tag{49}$$

Nambiar et al. (1992) noted that of the above-mentioned daughter size distributions, only the U-shape distribution is the most representative of the underlying physical phenomena. It stands to reason binary equal size break-up requires more energy than binary unequal size break-up. This was also supported by the experiments of Hesketh et al. (1987).

Due to the Lagrangian nature of the model, where each location of each individual bubble is known, information on the placement of the daughter bubbles is required. To the best of the authors' knowledge, no literature studies were performed regarding the locations of the daughter bubbles after a break-up event. There is also no relevant (video nor image) data available, which can be used to inspect the physical meaning of break-up locations. Hence, assumptions are to be made in the Euler–Lagrange framework regarding the placement of the two newly formed bubbles after a break-up event. For the placement of the resulting daughter bubbles the following is assumed. The centroid of the largest daughter bubble is placed on the same location as that of the parent bubble (x_0,y_0,z_0). The smallest daughter bubble is placed randomly around the centroid of the parent bubble at (x_1,y_1,z_1) with a center-to-center line distance between the two daughter bubbles (1 and 2) of

$$d_{12}=k\sqrt{(x_0-x_1)^2+(y_0-y_1)^2+(z_0-z_1)^2} \tag{50}$$

with $k=1.1$ to avoid immediate coalescence in a subsequent simulation time step. These assumptions are necessary since there is no literature nor relevant experimental data (video nor image) available that can be used to describe the physical meaning of break-up locations.

5. Numerical implementation

The Euler–Lagrange model is an in-house developed code written in C. A brief summary of the model is given here, while for more details the reader is referred to Darmana et al. (2006). This section mainly describes the numerical implementation of coalescence, break-up and interphase coupling. The coupled ordinary-differential equations of the individual bubbles are solved first. The liquid phase equations are solved using a modified version of the SIMPLE algorithm. The two-way coupling between the phases is treated in a linear implicit fashion.

5.1. Liquid phase flow field

The liquid phase flow field is calculated by solving the volume-averaged Navier–Stokes equations (Eqs. (3) and (4)) on an Eulerian grid using a fixed time step Δt_l. The equations are closed using the subgrid scale model by Vreman (2004) for turbulence modeling.

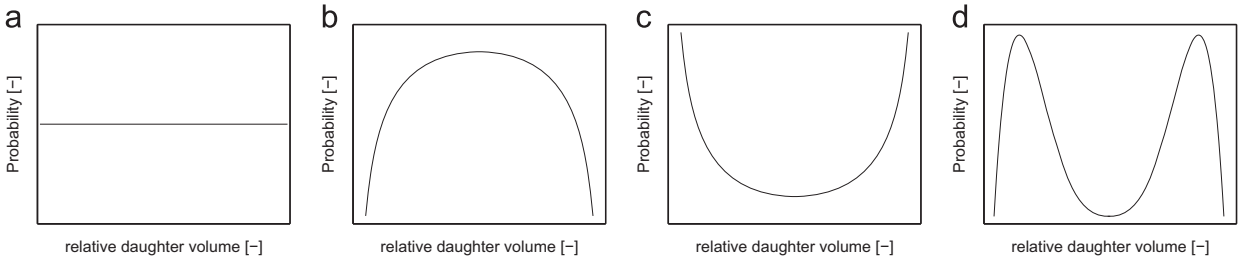

Fig. 2. Shapes of probable daughter bubble size distribution. (a) Uniform, (b) bell-shape, (c) U-shape and (d) M-shape.

5.2. Bubble dynamics

The equations for the displacement (Eq. (5)) of the individual bubbles are solved using explicit time advancing. The time step is Δt_b, which is a fixed fraction of Δt_l. Solving the equation during the bubble time step involves interpolation of the liquid velocity and local void fraction (for the drag force, virtual mass force and wall force calculations), pressure gradient (for the pressure force), and vorticity (for the lift force) to the bubble location. The interpolation is performed via the interphase coupling kernel, which is described in a later section. Within each bubble time step, the velocity of the bubbles is assumed to change only due to binary collisions between bubbles.

5.3. Collision/coalescence

Subsequently, after the calculation of the bubble velocity during the bubble time step, bubbles are moved by taking into account the interactions between bubbles or between bubbles and confining walls. Utilizing the hard-sphere model by Hoomans et al. (1996), movement of the bubbles is event-based. Bubble–wall interactions are treated as perfect elastic collisions, while for a bubble–bubble collision event, depending on the coalescence constraint either coalescence or a collision takes place.

As illustrated in Fig. 3, when the contact time is less than the film drainage time ($t_{\text{contact}} < t_{\text{drainage}}$) coalescence will not occur and the bubbles will bounce off each other. Momentum is exchanged and while the tangential component of the bubble velocity does not change, the normal component is changed according to the following relation:

$$\mathbf{v}_1^* = 2\frac{m_1\mathbf{v}_1 + m_2\mathbf{v}_2}{m_1+m_2} - \mathbf{v}_1 \quad \text{and} \quad \mathbf{v}_2^* = 2\frac{m_1\mathbf{v}_1 + m_2\mathbf{v}_2}{m_1+m_2} - \mathbf{v}_2 \tag{51}$$

In the other case as shown in Fig. 4, if $t_{\text{contact}} \geq t_{\text{drainage}}$, coalescence will occur and the properties of the newly formed bubble are calculated according to

$$V^* = V_1 + V_2; \quad \mathbf{r}^* = \frac{\mathbf{r}_1 m_1 + \mathbf{r}_2 m_2}{m^*} \quad \text{and} \quad \mathbf{v}^* = \frac{\mathbf{v}_1 m_1 + \mathbf{v}_2 m_2}{m^*} \tag{52}$$

5.4. Break-up

During the bubble time step, before the evaluation of the equation of motion, each individual bubble is evaluated on the basis of the break-up criteria. This corresponds to a evaluation frequency of $h_{bu} = 1/\Delta t_b$. If $\text{We} > \text{We}_{\text{crit}}$, the bubble break-up event takes place (see Fig. 5). Following literature models, binary break-up is assumed and the parent bubble breaks up into two daughter bubbles. For the calculation of the break-up fraction f_{bv}, either one of the earlier presented daughter size distribution can be selected (Table 2).

As mentioned before, assumptions are to be made regarding the locations of the daughter bubbles. The daughter bubble with the largest volume is placed at the original position of the parent bubble. Around this daughter bubble, the daughter bubble with the smallest volume is placed randomly with a specified distance between the center lines of the two bubbles. Positioning is done in such a way that no overlap with the surrounding bubbles results. The properties of the newly formed daughter bubbles are given in Table 3.

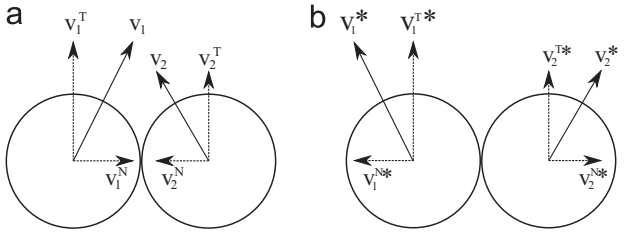

Fig. 3. Collision and bounce off. (a) Before collision and (b) after collision.

5.5. Interphase coupling

As mentioned earlier, the bubbles and the liquid phase are coupled through the liquid volume fraction α_l and the interphase momentum transfer rate Φ. Since both phases are defined in different reference frames (i.e. Lagrangian and Eulerian), a mapping technique is employed to correlate the two reference frames. This technique maps the Lagrangian bubble quantities to the Eulerian grid, which are required as closure for the liquid phase equations, and vice versa. For example, in order to evaluate the interphase momentum transfer rate from the liquid to a specific bubble, all the liquid phase quantities (i.e. pressure and velocity components) have to be available at the center of mass position of the bubble. Using a mapping technique, these local liquid properties are calculated from the values of the volume averaged liquid properties at the grid nodes surrounding the bubble under consideration.

The mapping technique depends on two parameters: the template function and the mapping window. These parameters are schematically illustrated in Fig. 6. The template function is constructed around the center of mass of the bubble b. In any computational cell j the integral of this function, $\int_{\Omega_j}\omega(b)\,d\Omega$ represents the influence of bubble b on cell j, but also the influence of the Eulerian value in cell j on bubble b. The integral is evaluated as follows:

$$\int_{\Omega_j}\omega(b)\,d\Omega = \int_{\Omega_{j,z}}\int_{\Omega_{j,y}}\int_{\Omega_{j,x}}\omega(x-x_b)\omega(y-y_b)\omega(z-z_b)\,dx\,dy\,dz \tag{53}$$

where $\omega(x_i - x_{b,i})$ is the template function that is identical for each of the three coordinate directions.

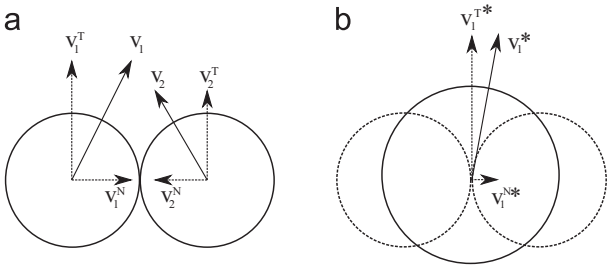

Fig. 4. Collision and coalescence. (a) Before coalescence and (b) after coalescence.

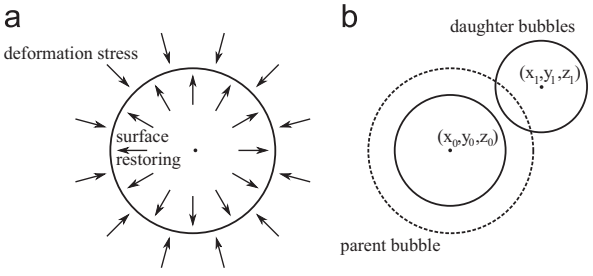

Fig. 5. Illustration of the daughter bubble locations after break-up. (a) Before break-up and (b) after break-up.

Table 2
List of selected critical Weber values.

System	Author	Critical Weber number	Remarks
Turbulent pipe flows	Walter and Blanch (1986) and Hesketh et al. (1987)	$We_{crit} = 5.9(\mu_l/\mu_g)^{1/6}$, $We_{crit} = 1.1(\rho_l/\rho_g)^{1/3}$	The conditions within pipe flow are not simple. First, turbulence is not the only cause of deformation due to the existence of a large mean-velocity gradient near the wall. Second, turbulence is not homogeneous. By using a scaling derived from the theory by Hinze (1955), some break-up criteria can be derived.
Microgravity conditions	Risso and Fabre (1998)	$We_{crit} \approx 2.7$–2.8	The break-up process of a single bubble is analyzed using a turbulent axisymmetric jet discharged into a closed tube. With the set-up a turbulent zone is obtained, where the fluctuations are large compared to the mean velocity (intense turbulence in the absence of a significant mean motion). Experiments are conducted under microgravity conditions to exclude buoyancy effects.
Balancing drag and buoyancy	Senhaji (1993)	$We_{crit} \approx 0.25$	Air bubbles in a uniform turbulent down flow were studied. In the experiment the mean liquid velocity (0.3 m/s) was chosen such that the drag force exerted on the bubble balances the buoyancy force. The turbulence was generated by an upstream oscillating grid.
Turbulent upward jet	Sevik and Park (1973)	$We_{crit} \approx 2.5$	The phenomenon of bubbles injected in the axis of a turbulent upward jet was studied. It was suggested that in the jet experiment, turbulence is not the single cause of bubble break-up.
Acceleration induced bubble break-up	Kolev (2007)	$We_{crit} \approx 12$	According to the author, this is the most frequently used value for the hydrodynamic stability in two-phase literature.

Table 3
Properties of the daughter bubbles, respectively 1 and 2, resulting from a break-up event of the parent bubble 0.

Daughter bubble	1	2
Volume	$V_1 = f_{bv} V_0$	$V_2 = (1 - f_{bv}) V_0$
Position	$\mathbf{r}_1 = \mathbf{r}_0$	$\mathbf{r}_2 = \mathbf{r}_0 + \Delta\mathbf{r}$
Velocity	$\mathbf{v}_1 = \mathbf{v}_0$	$\mathbf{v}_2 = \mathbf{v}_0$

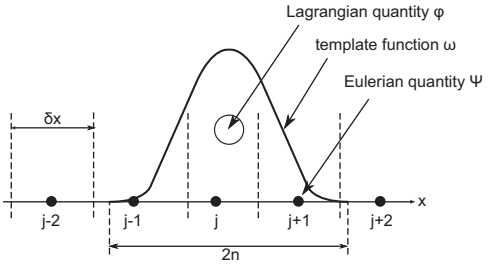

Fig. 6. Illustration of one-dimensional Lagrangian and Eulerian two-way coupling using a template window function.

Peskin (1977) proposed Gaussian functions, while Kitagawa et al. (2001) use a sine-wave function. In the present study a clipped fourth-order polynomial function following the work of Deen et al. (2004) is used:

$$\omega(x_i - x_{b,i}) = \frac{15}{16}\left[\frac{(x_i - x_{b,i})^4}{n^5} - 2\frac{(x_i - x_{b,i})^2}{n^3} + \frac{1}{n}\right]; \quad -n \le (x_i - x_{b,i}) \le n \tag{54}$$

with $2n$ the width of the mapping window. The Eulerian quantity $\Psi(j)$ of cell j is calculated from the Lagrangian quantity $\psi(b)$ of bubble b using the Lagrange to Euler mapping:

$$\Psi(j) = \frac{1}{V_{cell}} \sum_{\forall b \in B} \psi(b) \int_{\Omega_j} \omega(b)\, d\Omega \tag{55}$$

Vice versa, the Lagrangian quantity $\psi(b)$ of bubble b is calculated from the Eulerian quantity $\Psi(j)$ cell j using the Euler to Lagrange mapping:

$$\psi(b) = \sum_{\forall j \in C} \Psi(j) \int_{\Omega_j} \omega(b)\, d\Omega \tag{56}$$

6. Simulation domain

Simulations are performed for a square bubble column set-up for the air–water system. The column has a square cross-section ($W \times D$) of 0.15×0.15 m^2 and a height (L) of 0.45 m. Air was introduced into the system through the bottom of the column via gas injection points. The gas inlet consists of 7×7 points, which are positioned in the center of the bottom plane of the column with a square pitch of 6.25 mm. The diameter of bubbles entering the column is set to 4 mm as has been experimentally observed by Deen et al. (2001). The gas inlet points and the simulation domain are illustrated in Fig. 7 with the imposed boundary conditions according to the flag matrix concept by Kuipers et al. (1993). The definitions of the flags are listed in Table 4. For computations an equidistant numerical grid of $30 \times 30 \times 90$ and a fixed time step for the flow solver of 1.0×10^{-3} s are used. Earlier simulations performed by Darmana et al. (2005) and present simulations using grids ranging from $20 \times 20 \times 60$ to $40 \times 40 \times 120$ reveal that this configuration gives a grid and time step independent solution. The simulated time is set to 120 s, of which the first 20 s are discarded due to start-up effects.

A snapshot of the resulting bubble sizes in the simulated square bubble column is shown in Fig. 8. This involves a simulation with coalescence and break-up at a superficial gas velocity of 2 cm/s.

7. Results and discussion

Several simulations were performed with different parameter values to study their effect on the resulting BSD. The parameters, which are varied, are:

- critical break-up values: We_{crit}
- daughter size distributions: uniform, Bell-shape, U-shape and M-shape.
- superficial gas velocities: 1, 2 and 3 cm/s.

In order to evaluate the effect of each parameter, one simulation is chosen as the basis for comparison. In the base case we used a

superficial gas velocity of 2 cm/s, a break-up constraint $We_{crit} = 1$ and the U-shape daughter size distribution. In all other simulations we varied only one parameter as compared to the base case.

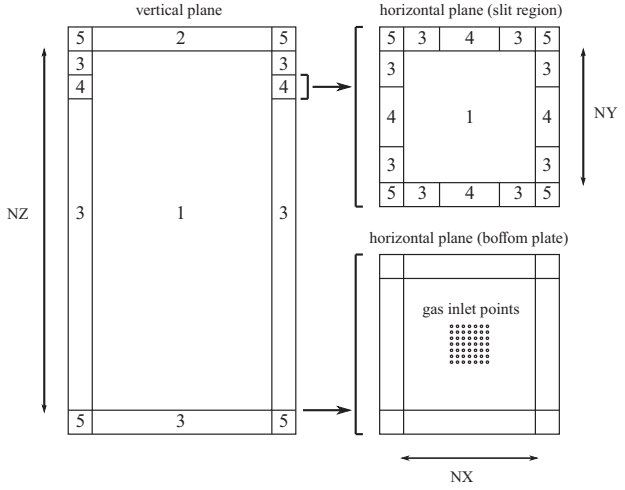

Fig. 7. Schematic overview of the numerical configuration of the simulated square bubble column.

Table 4
Definition of the flag boundary conditions.

Flag	Boundary conditions
1	Interior cell, no boundary conditions specified
2	Impermeable wall, free slip boundary
3	Impermeable wall, no slip boundary
4	Prescribed pressure cell, free slip boundary
5	Corner cell, no boundary conditions specified

7.1. Effect of critical Weber value

Fig. 9 shows the overall BSDs, which were obtained from the complete bubble column volume. Simulations were performed with different critical Weber values as break-up criteria at a superficial gas velocity of 2 cm/s. Note that in the simulation with $We_{crit} = \infty$ there is no bubble break-up. The large peaks at 4 mm originate from the inlet bubble diameter. These are the bubbles that did not coalesced into larger bubbles or broken up to smaller bubbles. All other peaks for bubble diameters > 4 mm belong to coalesced bubbles, corresponding to a multitude of the inlet bubble volume. For example the peak at 5.04 mm is the result of the coalescence of two equal-sized bubbles with a diameter of 4 mm. The following peak at 5.74 mm results from the coalescence of a bubble with a diameter of 4 mm and a bubble with a diameter of 5.04 mm. The next peak at 6.30 mm is from the coalescence of two equal-sized bubbles with a diameter of 5.04 mm. This phenomenon keeps on repeating for the following peaks. A decrease of We_{crit} results in all peaks to widen, since there is more break-up of bubbles > 4 mm. As can be seen from the plot, the number of bubbles < 4 mm increases due to lowering the We_{crit}. The mean bubble diameter and the standard deviation are listed in Table 5. The standard deviation appears not to depend on We_{crit}.

To illustrate the average coalescence and break-up rates, a cross-sectional plane is given in Fig. 10. The coalescence rate is very high near the bubble inlet region. In this lower region, the number of bubbles is high and collisions are more likely to occur than in the higher regions of the column.

The bubble break-up rate is the highest at the bubble inlet and at the top of the bubble column. Since the incoming bubbles experience large turbulent stresses, probability for break-up is very high at the bubble inlet. At the top of the bubble column the liquid flow is forced to exit and enter the column through the pressure outlets in the slits (see Fig. 8). The change of liquid flow direction causes bubbles to experience large shear stresses.

Fig. 11 shows the change of the BSD as a function of height. The column is divided into 5 sections along the height and for each section the BSD is calculated. At the lower sections, there are more small bubbles $d_b \leq 4$ mm than large bubbles $d_b > 4$ mm. In the

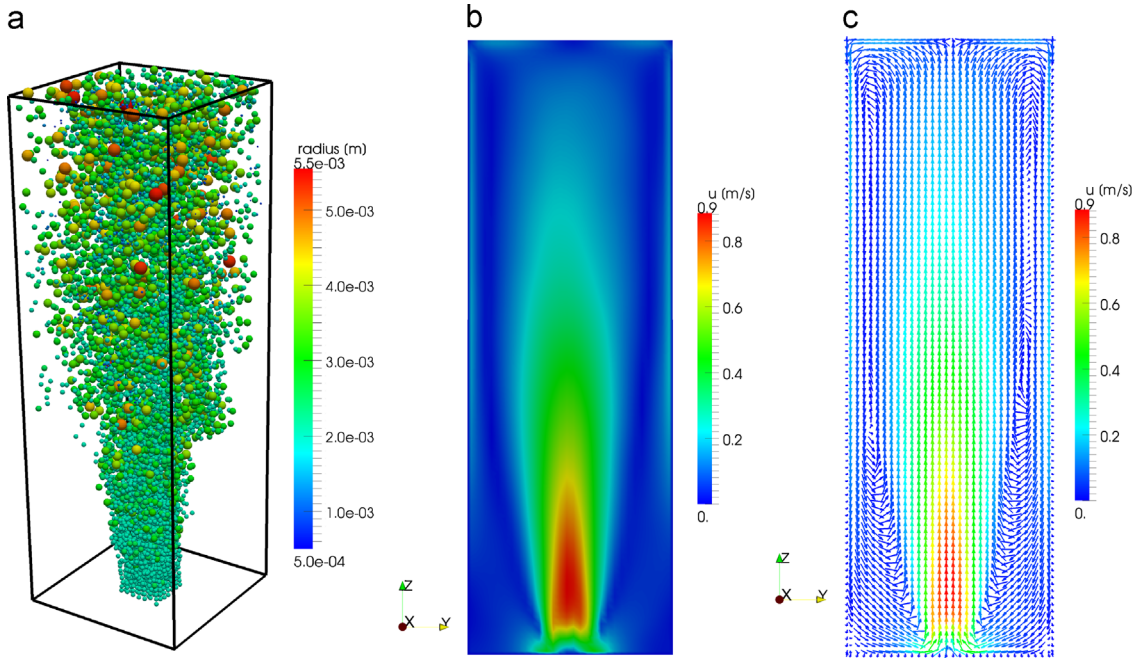

Fig. 8. Euler–Lagrange simulation with coalescence and break-up ($We_{crit} = 12\zeta$) at a superficial gas velocity of 2 cm/s: (a) three-dimensional snapshot, (b) time-averaged velocity magnitude and (c) time-averaged velocity vectors of the liquid flow field across the center plane of the bubble column.

higher sections of the column, there is a decrease of small bubbles and an increase of large bubbles. At the exit section of the column, the peak of the inlet bubble diameter has disappeared.

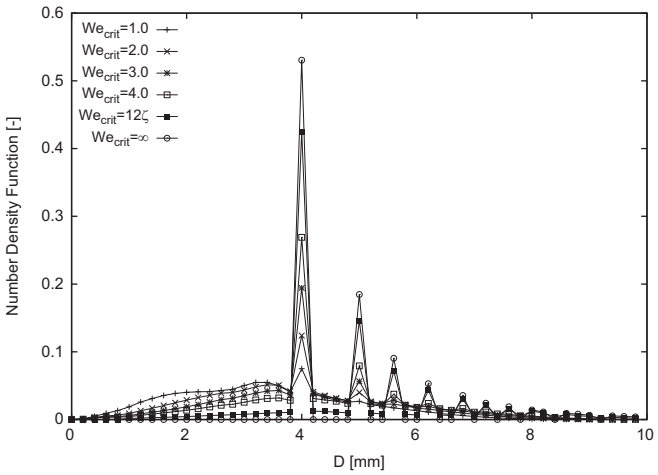

Fig. 9. Effect of critical Weber value (1, 2, 3, 4 and 12ζ) on the overall BSD of the simulations with a superficial gas velocity of 2 cm/s.

Table 5
The mean and standard deviation of the bubble diameter for the simulations with a superficial gas velocity of 2 cm/s and a critical Weber value range of 1, 2, 3, 4, 12ζ and ∞.

We_{crit}	d_{mean} (cm)	d_{std} (cm)
1	2.7	1.5
2	2.7	1.5
3	3.5	1.6
4	3.7	1.7
12ζ	4.2	1.6
∞	4.8	1.5

7.2. Effect of daughter bubble size distribution

Fig. 12 illustrates the effect of using different PDFs for the daughter size distribution (see Fig. 2). The large peak, which has the same value for all PDF shapes, corresponds to the inlet bubble diameter of 4 mm and the smaller peak at 5 mm is the result of coalescence of two inlet bubbles. As expected, the bell-shape PDF has the least small bubbles and the most bubbles with diameters between 2 mm and 4 mm. This is due to its low probability of generating small daughter bubbles and high probability for equal volume break-up. Compared with the bell-shape PDF, the uniform shape PDF has more small bubbles and less bubbles with diameters between 2 mm and 4 mm. The M-shape PDF lies within these two results. The U-shape PDF has the largest amount of small bubbles and also the lowest amount of bubbles with diameters between 2 mm and 4 mm. All these trends are in line with the shape of the daughter PDFs.

7.3. Effect of superficial gas velocity

Fig. 13 shows the overall BSD of simulations for different superficial gas velocity, respectively 1, 2 and 3 cm/s. The critical Weber value of the break-up model was set to 1 and an U-shaped daughter size distribution was used. For each of the velocities, the peak of the inlet bubble size is quite high, as well as the harmonic peaks belonging to the coalescence of inlet bubbles. By increasing the v_{sup} from 1 to 2 cm/s the overall BSD tends to smooth out. An increase of the amount of bubbles with diameters less than the inlet bubble size shows that there is an increase of bubble break-ups. Increasing the v_{sup} from 2 to 3 cm/s shows an increase of the amount of bubbles with diameters < 1.8 mm and a decrease of the amount of bubbles with diameters > 1.8 mm. This could be due to the increased local gas hold-up, where the distance between neighboring bubbles is very small. The bubble number density increases, because of the increased superficial gas velocity. The increased number density leads to less free space for daughter bubbles to be placed after a break-up event. Only small daughter

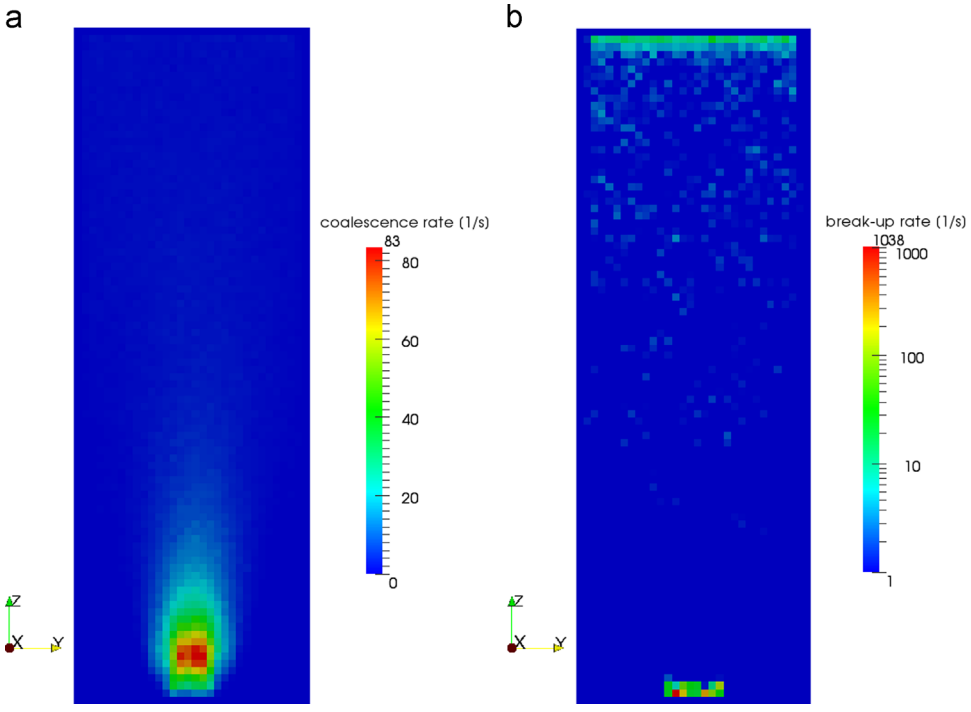

Fig. 10. Coalescence and break-up rates at a cross-sectional plane of the simulation with a superficial gas velocity of 2 cm/s and a critical Weber value of 1. The break-up rate is given in `log` scale. (a) Coalescence and (b) break-up.

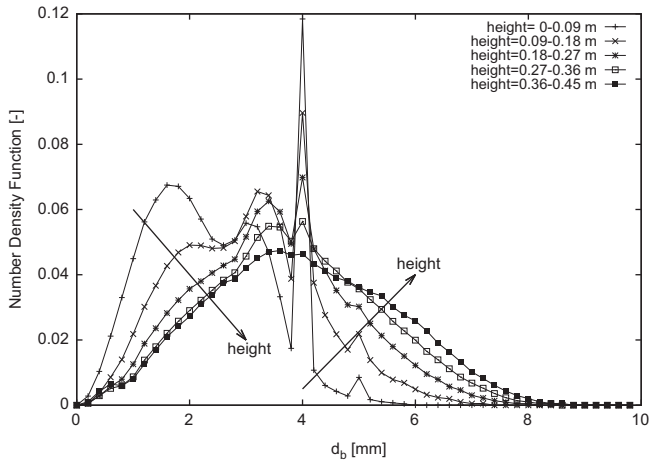

Fig. 11. Evolution of the local BSD across different height sections of the simulation with a superficial gas velocity of 2 cm/s and a critical Weber value of 1.

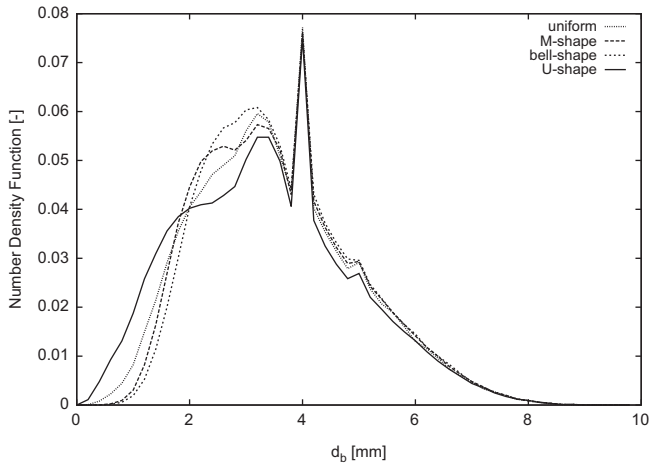

Fig. 12. Effect of different daughter bubble size distributions on the overall BSD of the simulations with a superficial gas velocity of 2 cm/s and a critical Weber value of 1.

bubbles can be placed in the available space in order to avoid overlap with neighboring bubbles. The used U-shaped daughter size distribution also contributes to the large amount of small bubbles.

The integral gas hold-up and the number of bubbles are given in Tables 6 and 7. These tables also show the corresponding values of simulations without coalescence and break-up and only coalescence. As expected, the simulation without coalescence and break-up modeling has the largest integral gas hold-up and the simulation with only coalescence has the lowest integral gas hold-up. If there is no coalescence and break-up, all bubbles have the same size and have similar residence time within the column. Due to coalescence of bubbles, larger bubbles exit the column faster and have a shorter residence time. In between these two values lie the integral gas hold-up of the simulation with coalescence and break-up. The difference between the simulations without coalescence and break-up and only coalescence is also reflected in the number of bubbles residing in the column. Due to coalescence, the number of bubbles is reduced. For the simulation with coalescence and break-up, it as expected that the number of bubbles would be very large due to the break-up of bubbles into a large number of smaller bubbles.

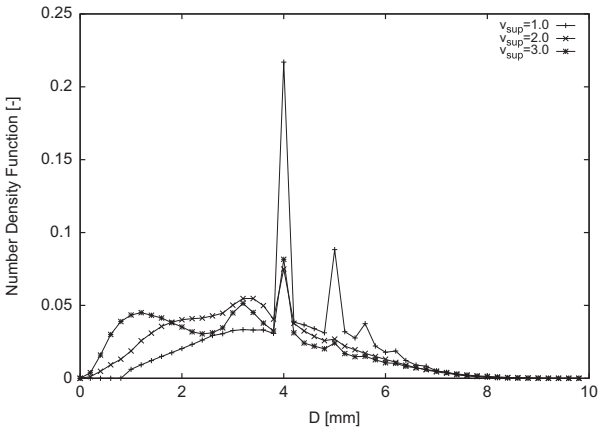

Fig. 13. Effect of superficial gas velocity on the overall BSD of the simulations with a critical Weber value of 1 and a U-shape daughter bubble size distribution.

Table 6
Integral gas hold-up values of the simulations with superficial gas velocities of 1, 2 and 3 cm/s, with and without coalescence and break-up modeling. For the break-up model a critical Weber value of 1 and a U-shaped daughter size distribution are used.

v_{sup} (cm/s)	Integral gas hold-up α_g		
	No coalescence and no break-up	Only coalescence	Coalescence and break-up
1	2.04	1.73	1.96
2	4.34	3.65	4.30
3	7.40	5.68	6.54

Table 7
Number of bubbles of the simulations with superficial gas velocities of 1, 2 and 3 cm/s, with and without coalescence and break-up modeling. For the break-up model a critical Weber value of 1 and a U-shaped daughter size distribution are used.

v_{sup} (cm/s)	Number of bubbles		
	No coalescence and no break-up	Only coalescence	Coalescence and break-up
1	8400	2800	8400
2	18 000	6400	30 600
3	32 000	9800	65 100

8. Conclusions

A complete coalescence and break-up model has been formulated and implemented in the Euler–Lagrange framework. The break-up model consists of a break-up constraint and a daughter size distribution. The break-up constraint is derived on the basis of the underlying concepts of literature break-up models for the Population Balance Equation (PBE). The constraints of the PBE break-up models can be written in terms of a dimensionless Weber number. Hence, as a constraint for the deterministic Euler–Lagrange framework, an individual bubble breaks up if $We > We_{crit}$. The critical value depends on the bubble aspect ratio E_b and the Eö number.

Daughter size distribution in the literature studies can be categorized according to their shapes. From these shapes, the U-shape distribution seems to be more representative of the underlying physical concepts of bubble break-up. Since the energy requirement for binary equal size break-up is larger than unequal size break-up, it is easier for a small daughter bubble to be separated from the large parent bubble.

Both the break-up constraint and the daughter size distribution are implemented in the deterministic Euler–Lagrange framework. With this Euler–Lagrange model, the BSD of turbulent bubbly flows can be investigated. The BSD is a direct result of the coalescence and break-up of the individual bubbles within the simulation.

A numerical study of the parameters of the break-up model in an Euler–Lagrange model is presented here for the bubbly flow in a square column. Changes were made in values of the critical Weber number We_{crit}, the daughter size distribution β and the superficial gas velocity v_{sup}.

A decrease of We_{crit} shows a significant change in the overall BSD with many more small bubbles due to break-up. Increased break-ups tends to smoothen the BSD.

Changing the shape of the daughter size distribution results in some minor changes of the overall BSD, which inherits features of the chosen shape. For example, the difference between the U-shape and Bell-shape daughter distributions is that with the Bell-shape there are more smaller bubbles.

Increasing the superficial gas velocity from 1 to 2 cm/s and from 2 to 3 cm/s shows a smoother overall BSD. For the latter, the overall BSD has a more profound increase in the amount of small bubbles. This can be caused by the increase of local gas hold-up in the column, which results in less space to place daughter bubbles after a break-up event. Only small bubbles can be placed in the available space.

Nomenclature

A	area, (m^2)
$B, c_{1\ldots6}, k, p$	model parameters (dimensionless)
C	model coefficient (dimensionless)
D	depth (m)
d	diameter (m)
E_b	bubble aspect ratio (d_z/d_x) (dimensionless)
E	energy (kg m^2 s^2)
$\mathbf{F}$	force (N)
f_{bv}	volumetric break-up fraction (dimensionless)
$\mathbf{g}$	gravitational acceleration (m^2/s)
H	height (m)
h_{bu}	arrival frequency of eddies (1/s)
h_{coll}	collision frequency between two bubbles (m^3/s)
L	length (m)
m	mass (kg)
min	minimum
N	number of bubbles
$\mathbf{n}$	normal vector (dimensionless)
n	mapping window size (m)
P	pressure (N/m^2)
$\mathbf{r}$	location (m)
r	radius (m)
S	perimeter (m)
t	time (s)
$\mathbf{u}$,u	liquid velocity (m/s)
$\mathbf{v}$,v	bubble/gas/droplet velocity (m/s)
V	volume (m^3)
W,w	width (m)
x, y, z	x, y, z coordinates (m)
Δr	displacement (m)
Δt	time step (s)
Δx	grid size (m)

Greek letters

α	phase fraction (dimensionless)
β	daughter size distribution (dimensionless)
ε	turbulent dissipation rate (m^2/s^3)
λ	eddy length scale (m)
μ	viscosity (Pa s)
Ω	mapping domain (m^3)
ω	template function (dimensionless)
Φ	source term of momentum exchange (N/m^3)
Ψ	Eulerian quantity (dimensionless)
ψ	Lagrangian quantity (dimensionless)
ρ	density (kg/m^3)
σ	surface tension coefficient (N/m)
$\boldsymbol{\tau}$	stress tensor (N/m^2)
Γ	gamma function (dimensionless)
γ_{bu}	break-up efficiency (dimensionless)
γ_{co}	coalescence efficiency (dimensionless)
Θ_{bu}	break-up frequency (1/s)
Θ_{co}	coalescence frequency (m^3/s)
θ	film thickness (m)
Υ	random value (dimensionless)
ζ	correction factor (dimensionless)

Subscripts and superscripts

0,1,2	initial, first, second
b	bubble
bu	break-up
co	coalescence
$coll$	collision
crit	critical
D	drag
d	distorted
eq	equivalent
f	final
G	gravity
g	gas phase
i,j	indices
kin	kinetic
L	lift
l	liquid phase
max	maximum
min	minimum
N	normal direction
P	pressure
rel	relative
s	surface
std	standard deviation
T	tangential direction
t	turbulent
VM	virtual mass
W	wall
xy, z	in x, y, z direction

Abbreviations

BSD	bubble size distribution
PBE	population balance equation
PDF	probability density function
SIMPLE	semi-implicit method for pressure linked equations

Dimensionless numbers

Eö	Eötvös number $g_z d^2 \rho_l/\sigma$

Mo	Morton number $g_z\mu_l^4\Delta\rho/(\rho_l^2\sigma^3)$
Oh	Ohnesorge number $(\mu_g/\sqrt{\rho_g\sigma d})$
Re	Reynolds number $\rho v\, d/\mu_l$
We	Weber number $\rho_l\overline{\delta u^2(d)}d/\sigma$

Acknowledgments

This project is part of the Industrial Partnership Program "Fundamentals of Heterogeneous Bubbly Flow", which is funded by FOM, AkzoNobel, DSM, Shell and TataSteel.

Appendix A. Derivation of the break-up constraint

The derivation of ζ in Section 4.1.2 is given here. ζ is a correction factor for the surface area of a bubble (calculated using d_{eq}) to account for the actual Eötvös number/aspect ratio E_b. Consider an ellipsoidal bubble with different radii $r_x \neq r_y \neq r_z$, $r_y \geq r_x$ and $d_z = (1+B)r_z$ (see Fig. A1). To relate each of the radii to the equivalent diameter the aspect ratio and volume of the bubble are used. The bubble aspect ratio E_b is defined as the maximum vertical dimension divided by the maximum horizontal dimension:

$$E_b = \frac{(1+B)}{2C}\cdot\frac{r_z}{r_x} \tag{57}$$

The volume of an ellipsoidal bubble is equal to the sum of the volume of the upper half and the lower half of the hemisphere of the bubble:

$$\frac{1}{2}\cdot\frac{4}{3}\pi\cdot r_x r_y r_z + \frac{1}{2}\cdot\frac{4}{3}\pi\cdot r_x r_y B r_z = \frac{4}{3}\pi\frac{D_{eq}^3}{8} \tag{58}$$

$$4\cdot(1+B)\cdot r_x r_y r_z = D_{eq}^3 \tag{59}$$

From Eq. (57)

$$r_z = \frac{2E_bC}{1+B}\cdot r_x \tag{60}$$

Substitution in Eq. (59) gives

$$4\cdot(1+B)\cdot r_x\cdot(C\cdot r_x)\cdot\left(\frac{2E_bC}{1+B}\cdot r_x\right) = D_{eq}^3 \tag{61}$$

$$\rightarrow r_x = \frac{1}{2}\cdot E_b^{-1/3}\cdot C^{-2/3}\cdot D_{eq} \tag{62}$$

$$\rightarrow r_y = \frac{1}{2}\cdot E_b^{-1/3}\cdot C^{1/3}\cdot D_{eq} \tag{63}$$

$$\rightarrow r_z = \frac{1}{1+B}\cdot E_b^{2/3}\cdot C^{1/3}\cdot D_{eq} \tag{64}$$

Following the work of Klamkin (1971), an approximate equation to calculate the surface area of an ellipsoidal bubble is

$$A = 4\pi\left(\frac{r_x^p r_y^p + r_x^p r_z^p + r_y^p r_z^p}{3}\right)^{1/p} \tag{65}$$

with $p=1.6075$. Substitution of Eqs. (62)–(64) in Eq. (65) results in

$$A_{upper} = \pi D_{eq}^2 \times\left(\frac{\left(\frac{1}{2}\right)^p\cdot E_b^{-2/3p}\cdot C^{-1/3p} + \left(\frac{1}{1+B}\right)^p\cdot E_b^{1/3p}\cdot C^{-1/3p} + \left(\frac{1}{1+B}\right)^p\cdot E_b^{1/3p}\cdot C^{2/3p}}{3}\right)^{1/p} \tag{66}$$

Multiplying both the denominator and enumerator with $E_b^{2/3p}\cdot C^{1/3p}\cdot(1+B)^p$:

$$A_{upper} = \pi D_{eq}^2\cdot\left(\frac{(\frac{1}{2})^p\cdot(1+B)^p + E_b^p + E_b^p\cdot C^p}{3\cdot E_b^{2/3p}\cdot C^{1/3p}\cdot(1+B)^p}\right)^{1/p} \tag{67}$$

Similar to the upper surface area A_{upper}, the lower surface area A_{lower} is derived with $|B|\cdot r_z$. The absolute of $|B|$ is to account for $-1<B<0$ (cap regime).

$$A_{lower} = \pi D_{eq}^2\cdot\left(\frac{(\frac{1}{2})^p\cdot(1+B)^p + |B|^p\cdot E_b^p + |B|^p\cdot E_b^p\cdot C^p}{3\cdot E_b^{2/3p}\cdot C^{1/3p}\cdot(1+B)^p}\right)^{1/p} \tag{68}$$

The total surface area is

$$A = A_{upper} + A_{lower} \tag{69}$$

$$A = \pi D_{eq}^2\cdot\left(\frac{(\frac{1}{2})^p\cdot(1+B)^p + E_b^p + E_b^p\cdot C^p}{3\cdot E_b^{2/3p}\cdot C^{1/3p}\cdot(1+B)^p}\right)^{1/p} + \pi D_{eq}^2 \times\left(\frac{(\frac{1}{2})^p\cdot(1+B)^p + |B|^p\cdot E_b^p + |B|^p\cdot E_b^p\cdot C^p}{3\cdot E_b^{2/3p}\cdot C^{1/3p}\cdot(1+B)^p}\right)^{1/p} \tag{70}$$

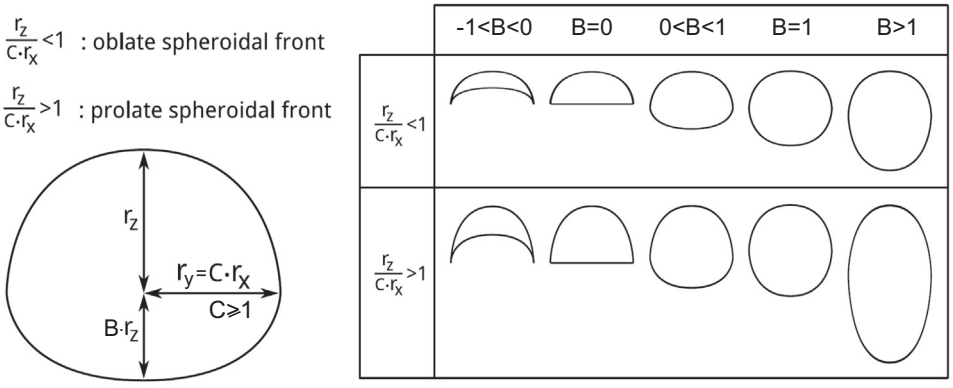

Fig. A1. Various bubble shapes in a two-dimensional plane (Tomiyama, 2004).

The surface area can be written as

$$A = \pi D_{eq}^2 \cdot \zeta^{-1} \tag{71}$$

with:

$$\zeta = \left(\left(\frac{(\frac{1}{2})^p \cdot (1+B)^p + E_b^p + E_b^p \cdot C^p}{3 \cdot E_b^{2/3p} \cdot C^{1/3p} \cdot (1+B)^p} \right)^{1/p} + \left(\frac{(\frac{1}{2})^p \cdot (1+B)^p + |B|^p \cdot E_b^p + |B|^p \cdot E_b^p \cdot C^p}{3 \cdot E_b^{2/3p} \cdot C^{1/3p} \cdot (1+B)^p} \right)^{(1/p)} \right)^{-1} \tag{72}$$

The surface correction factor can be simplified with $C=1$ and $B=1 \rightarrow E_b = r_z/r_x$ and $r_z = E_b \cdot r_y = E_b \cdot r_x$:

$$\zeta = \left(\frac{1+2E_b^p}{3E_b^{2/3p}} \right)^{-1/p} \tag{73}$$

For a spherical bubble, $C=1$ and $E_b=1$ and $B=1 \rightarrow 1 = r_z/r_x$ and $r_z = r_y = r_x$

$$\zeta = 1 \tag{74}$$

References

Alopaeus, V., Koskinen, J., Keskinen, K.I., Majander, J., 2002. Simulation of the population balances for liquid–liquid systems in a non-ideal stirred tank. Part 2 – parameter fitting and the use of the multiblock model for dense dispersions. Chem. Eng. Sci. 57, 1815–1825.

Auton, T.R., 1987. The lift force on a spherical body in rotational flow. J. Fluid Mech. 197, 241–257.

Batchelor, G.K., 1951. Proc. Cambridge Phil. Soc. 47, 359.

Chatzi, E., Garrielides, A.D., Kiparissides, C., 1989. Generalized model for prediction of the steady-state drop size distributions in batch stirred vessels. Ind. Eng. Chem. Res. 28, 1704–1711.

Chatzi, E., Kiparissides, C., 1992. Dynamic simulation of bimodal drop size distributions in low-coalescence batch dispersion systems. Chem. Eng. Sci. 47, 445–456.

Chesters, A.K., 1991. The modeling of coalescence processes in fluid–liquid dispersions: a review of current understanding. Chem. Eng. Res. Des.: Trans. Inst. Chem. Eng. Part A 69, 259–270.

Coulaloglou, C.A., Tavlarides, L.L., 1977. Description of interaction processes in agitated liquid–liquid dispersions. Chem. Eng. Sci. 32, 1289–1297.

Darmana, D., Deen, N.G., Kuipers, J.A.M., 2005. Detailed modelling of hydrodynamics, mass transfer and chemical reactions in a bubble column using a discrete bubble model. Chem. Eng. Sci. 12, 3383–3404.

Darmana, D., Deen, N.G., Kuipers, J.A.M., 2006. Parallelization of an Euler–Lagrange model using mixed domain decomposition and a mirror domain technique: application to dispersed gas–liquid two-phase flow. J. Comput. Phys. 220 (1), 216–248.

Darmana, D., Henket, R.L.B., Deen, N.G., Kuipers, J.A.M., 2007. Detailed modelling of hydrodynamics, mass transfer and chemical reactions in a bubble column using a discrete bubble model: chemisorption of CO_2 into NaOH solution, numerical and experimental study. Chem. Eng. Sci. 62, 2556–2575.

Deen, N.G., Solberg, T., Hjertager, B.H., 2001. Large Eddy simulation of the gas–liquid flow in a square cross-sectioned bubble column. Chem. Eng. Sci. 56, 6341–6349.

Deen, N.G., van Sint Annaland, M., Kuipers, J.A.M., 2004. Multi-scale modeling of dispersed gas–liquid two-phase flow. Chem. Eng. Sci. 59, 1853–1861.

Delnoij, E., Lammers, F.A., Kuipers, J.A.M., van Swaaij, W.P.M., 1997. Dynamic simulation of dispersed gas–liquid two-phase flow using a discrete bubble model. Chem. Eng. Sci. 52 (9), 1429–1458.

Delnoij, E., Kuipers, J.A.M., van Swaaij, W.P.M., 1999. A three-dimensional CFD model for gas–liquid bubble columns. Chem. Eng. Sci. 54 (13–14), 2217–2226.

Hesketh, R.P., Etchells, A.W., Russell, T.W.F., 1987. Bubble size in horizontal pipelines. AIChE J. 33, 663.

Hinze, J.O., 1955. Fundamentals of hydrodynamic mechanism of splitting in dispersion processes. AIChE J. 1 (3), 289–295.

Hoomans, B.P.B., Kuipers, J.A.M., Briels, W.J., Van Swaaij, W.P.M., 1996. Discrete particle simulation of bubbles and slug formation in a two-dimensional gas-fluidized bed: a hard-sphere approach. Chem. Eng. Sci. 51 (1), 99–118.

Howarth, W.J., 1964. Coalescence of drops in a turbulent flowfield. Chem. Eng. Sci. 19, 33–38.

Kitagawa, A., Murai, Y., Yamamoto, F., 2001. Two-way coupling of Eulerian–Lagrangian model for dispersed multiphase flows using filtering functions. Int. J. Multiph. Flow 27 (12), 2129–2153.

Klamkin, M.S., 1971. Elementary approximations to the area of N-dimensional ellipsoids. Am. Math. Mon. 78 (3), 280–283.

Kolev, N.I., 2007. Multiphase Flow Dynamics 1: Fundamentals, 3rd ed. Springer, Berlin.

Kolmogorov, A.N., 1949. On the breakage of drops in a turbulent flow. Dokl. Akad. Navk. SSSR 66, 825–828.

Kuipers, J.A.M., van Duin, K.J., van Beckum, F.P.H., van Swaaij, W.P.M., 1993. Computer simulation of the hydrodynamics of a two dimensional gas-fluidized bed. Comp. Chem. Eng. 17, 839.

Lasheras, J.C., Eastwood, C., Martínez-Bazán, C., Montañés, J.L., 2002. A review of statistical models for the break-up of an immiscible fluid immersed into a fully developed turbulent flow. Int. J. Multiph. Flow 28, 247–278.

Lee, C.-H., Erickson, L.E., Glasgow, L.A., 1987. Bubble breakup and coalescence in turbulent gas–liquid dispersions. Chem. Eng. Commun. 59, 65–84.

Lee, C.H., Erickson, L.E., Glasgow, L.A., 1987. Dynamics of bubble size distribution in turbulent gas–liquid dispersions. Chem. Eng. Commun. 61, 181–195.

Lehr, F., Millies, M., Mewes, D., 2002. Bubble size distributions and flow fields in bubble columns. AIChE J. 48 (11), 2426–2443.

Liao, Y.X., Lucas, D., 2009. A literature review of theoretical models for drop and bubble breakup in turbulent dispersions. Chem. Eng. Sci. 64, 3389–3406.

Liao, Y.X., Lucas, D., 2010. A literature review on mechanisms and models for the coalescence process of fluid particles. Chem. Eng. Sci. 65, 2851–2864.

Luo, H., Svendsen, H.F., 1996. Theoretical model for drop and bubble breakup in turbulent dispersions. AIChE J. 42 (5), 1225–1233.

Martínez-Bazán, C., Montañés, J.L., Lasheras, J.C., 1999. On the break up of an air bubble injected into fully developed turbulent flow. Part 1. Breakup frequency. J. Fluid Mech. 401, 157–182.

Nambiar, D.K.R., Kumar, R., Das, T.R., Gandhi, K.S., 1992. A new model for the breakage frequency of drops in turbulent stirred dispersions. Chem. Eng. Sci. 47 (12), 2989–3002.

Narsimhan, G., Gupta, J.P., 1979. A model for transitional breakage probability of droplets in agitated lean liquid–liquid dispersions. Chem. Eng. Sci. 34, 257–265.

Peskin, C.S., 1977. Numerical analysis of blood flow in the heart. J. Comput. Phys. 25, 220–252.

Prince, M.J., Blanch, H.W., 1990. Bubble coalescence and break-up in air-sparged bubble columns. AIChE J. 36, 1485–1499.

Risso, F., Fabre, J., 1998. Oscillations and breakup of a bubble immersed in a turbulent field. J. Fluid Mech. 372, 323–355.

Roghair, I., Lau, Y.M., Deen, N.G., Baltussen, M., Slagter, M., Van Sint Annaland, M., Kuipers, J.A.M., 2011. On the drag force of bubbles in bubble swarms for intermediate and high Reynolds numbers. Chem. Eng. Sci. 66 (14), 3204–3211.

Sagert, N.H., Quinn, M.J., 1976. The coalescence of H_2S and CO_2 bubbles in water. Can. J. Chem. Eng. 54, 392–398.

Senhaji, R., 1993. Qualification globale du fractionnement d′une phase disperseé de faible viscosité en fonction des proprié tié s turbulentes de l′é coulement externe. (thesis), Ecole Centrale de Nantes.

Sevik, M., Park, S.H., 1973. The splitting of drops and bubbles by turbulent fluid flow. J. Fluids Eng. 95, 53–60.

Smagorinsky, J., 1963. General circulation experiment with the primitive equations. Mon. Weather Rev. 91, 99–165.

Sommerfeld, M., Bourloutski, E., Bröder, D., 2003. Euler/Lagrange calculations of bubbly flows with consideration of bubble coalescence. Can. J. Chem. Eng. 81 (3–4), 508–518.

Sovova, H., 1981. Breakage and coalescence of drops in a batch stirred vessel – II comparison of model and experiments. Chem. Eng. Sci. 36, 1567–1573.

Sungkorn, R., Derksen, J.J., Khinast, J.G., 2012. Euler–Lagrange modeling of a gas–liquid stirred reactor with consideration of bubble breakage and coalescence. AIChE J. 58, 1356–1370.

Tsouris, C., Tavlarides, L.L., 1994. Breakage and coalescence models for drops in turbulent dispersions. AIChE J. 40, 395–406.

Tomiyama, A., Matsuoka, T., Fukuda, T., Sakaguchi, T., 1995. A simple numerical method for solving an incompressible two-fluid model in a general curvilinear coordinate system. In: Seizawa, A., Fukano, T., Bataille, J. (Eds.), Advances in Multiphase Flow. Society of Petroleum Engineers, Inc., Elsevier, Amsterdam, pp. 241–252.

Tomiyama, A., Tamai, H., Zun, I., Hosokawa, S., 2002. Transverse migration of single bubbles in simple shear flows. Chem. Eng. Sci. 57, 1849–1858.

Tomiyama, A., 2004. Drag, lift and virtual mass forces acting on a single bubble. In: 3rd International Symposium on Two-Phase Flow Modelling and Experimentation Pisa, September 22–24.

Vreman, A.W., 2004. An Eddy-viscosity subgrid-scale model for turbulent shear flow: algebraic theory and applications. Phys. Fluids 16, 10.

Walter, J.F., Blanch, H.W., 1986. Bubble break-up in gas–liquid bioreactors – break-up in turbulent flows. Chem. Eng. J. Biochem. Eng. J. 32 (1), B7–B17.